Article

Weak, Broken, but Working—Intramolecular Hydrogen Bond in 2,2′-bipyridine

Ilya G. Shenderovich (ID)

Institute of Organic Chemistry, University of Regensburg, 93053 Regensburg, Germany; ilya.shenderovich@ur.de

Abstract: From an academic and practical point of view, it is desirable to be able to assess the possibility of the proton exchange of a given molecular system just by knowing the positions of the proton acceptor and the proton donor. This study addresses the difference between intramolecular hydrogen bonds in 2,2′-bipyridinium and 1,10-phenanthrolinium. Solid-state ^{15}N NMR and model calculations show that these hydrogen bonds are weak; their energies are 25 kJ/mol and 15 kJ/mol, respectively. Neither these hydrogen bonds nor N-H stretches can be responsible for the fast reversible proton transfer observed for 2,2′-bipyridinium in a polar solvent down to 115 K. This process must have been caused by an external force, which was a fluctuating electric field present in the solution. However, these hydrogen bonds are the grain that tips the scales precisely because they are an integral part of a large system of interactions, including both intramolecular interactions and environmental influence.

Keywords: non-covalent interactions; NMR; proton transfer; 1,10-phenanthroline; GIAO

1. Introduction

Non-covalent interactions make our world alive. Of particular importance, at least for biological systems, is hydrogen bonding. Among other things, this interaction is an almost indispensable initial step for the simplest molecular chemical reaction, and at the same time, the most important biological chemical reaction—the proton transfer reaction [1,2]. The rate of this reaction strongly depends on the distance between the proton acceptor and the proton donor groups, as well as on the deviation of the formed hydrogen bond from linearity. From an academic and practical point of view, it is therefore desirable to be able to assess the possibility of the proton exchange of a given molecular system with limited mobility just by knowing the position and mutual orientation of the proton acceptor and the proton donor. One of the ways to solve this problem is to study model systems for which the arrangement of these groups is similar but the characteristics of the hydrogen bond and associated proton exchange are different. 2,2′-bipyridine (BiPy) and 1,10-phenanthroline (Phen) represent a suitable model pair for such a study (Figure 1).
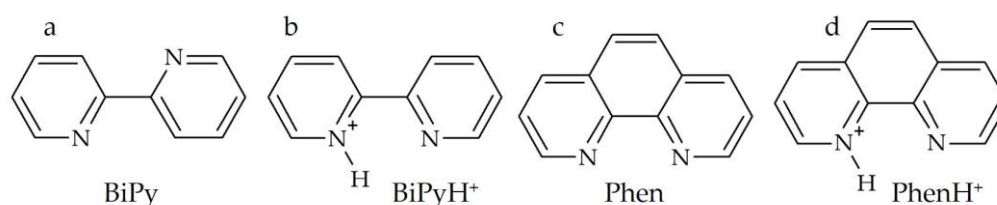

Figure 1. Substances studied in this work. (**a**) 2,2′-bipyridine (BiPy), (**b**) 2,2′-bipyridinium (BiPyH⁺), (**c**) 1,10-phenanthroline (Phen), (**d**) 1,10-phenanthrolinium (PhenH⁺).

Theoretical calculations show that both the *cis* and *trans* conformers of BiPy can be present in the gas phase and solutions [3]. The *trans* conformer is lower in energy, and the barrier for *cis/trans* interconversion is small. This conformer is planar in the gas [3]

and solid phases [4–6] but can be nonplanar in solutions [7]. When adsorbed onto silica, BiPy also adopts the *trans* conformation. [8]. In contrast, for 2,2′-bipyridinium (BiPyH$^+$), its *cis* conformer is the low-energy one in the gas phase [3], solution [9], and the solid state [10–16]. This conformer is planar in the gas phase [3] and, as an exception, in the solid state in the case of non-coordinating anions [17–25]. The N . . . N distance in these structures varies from 2.611 Å [10] to 2.727 Å [23]. A detailed examination suggested that the N . . . N distance is determined more by the crystal packing than by the planarity of the molecule itself [25].

BiPy can be doubly protonated. In this form, its conformation tends back to the *trans* orientation, and the torsion angle between its rings varies from 36° to 180° [23,26].

The most stable conformation of other bipyridines often depends on intramolecular interactions [27,28]. For BiPyH$^+$, the stabilization of the *cis* conformer is intuitively associated with the formation of an intramolecular hydrogen bond. In this regard, it is often compared with 1,10-phenanthrolinium (PhenH$^+$). Indeed, the fundamental coordination [11] and proton-accepting properties of BiPy and Phen are similar.

The N . . . N distances in Phen and PhenH$^+$ are about 2.71–2.74 Å [10,11,14,16,17,23,29,30]. Phen can be doubly protonated. In this form, the N . . . N distance is about 2.80–2.90 Å [31–36], and the planarity of the molecule can be somewhat distorted. This allows us to make the following assumptions. The molecular structure of Phen is flexible enough to accommodate intermolecular non-covalent interactions. This is evident from the possibility of the double protonation and some contraction in PhenH$^+$.

The difference between the intramolecular hydrogen bonds in BiPyH$^+$ and PhenH$^+$ has been addressed in the past. The following arguments were given as proof of the presence of a strong hydrogen bond in BiPyH$^+$. The ν(NH) stretching frequency at 10 K is 3147 cm^{-1}, while in PhenH$^+$, it is 3279 cm^{-1} [10]. A lower limit on the strength of the intramolecular hydrogen bond in BiPyH$^+$ was placed at 63 kJ/mol [3]. A fast reversible intramolecular hydrogen bond transfer in BiPyH$^+$ was observed in a polar solvent down to 115 K [9]. This process is consistent with the presence of a strong intramolecular hydrogen bond. However, all these arguments only do not contradict the presence of this interaction, but they do not allow us to evaluate its strength either numerically or in comparison with the hydrogen bond in PhenH$^+$. On the other hand, the difference between the N . . . N distances in BiPyH$^+$ and PhenH$^+$ is small. If we take into account that both bonds are nonlinear, then the difference between their energies can be insignificant.

This work has the following objectives: (i) to measure the ^{15}N NMR chemical shifts of BiPy, Phen, BiPyH$^+$, and PhenH$^+$ in the solid state and to compare these experimental values with theoretically calculated values to determine the correct hydrogen bond geometry in the condensed state; (ii) to estimate the energy of the intramolecular hydrogen bonds in BiPyH$^+$ and PhenH$^+$; (iii) to theoretically model the intramolecular proton transfer in BiPyH$^+$ and PhenH$^+$ to elucidate the most likely mechanism and barrier height.

2. Results and Discussion

2.1. Hydrogen Bond Geometry and Energy in BiPyH$^+$ and PhenH$^+$

2.1.1. Experimental ^{15}N NMR Chemical Shifts

Figure 2 shows the ^{15}N NMR spectra of polycrystalline samples of BiPy, Phen, BiPyH$^+$, and PhenH$^+$. The numerical values of the isotropic chemical shift, $\delta_{iso}(^{15}N)$, are collected in Table 1. The $\delta_{iso}(^{15}N)$ values of BiPy and Phen were similar in the solid state and in a solution of tetrahydrofuran. There are two structurally distinct molecules in the crystal structure of Phen [29,30]. The anisotropy of the chemical shift tensors of structurally different molecules is different, which results in the difference in their δ_{iso} and spinning sideband patterns [37].
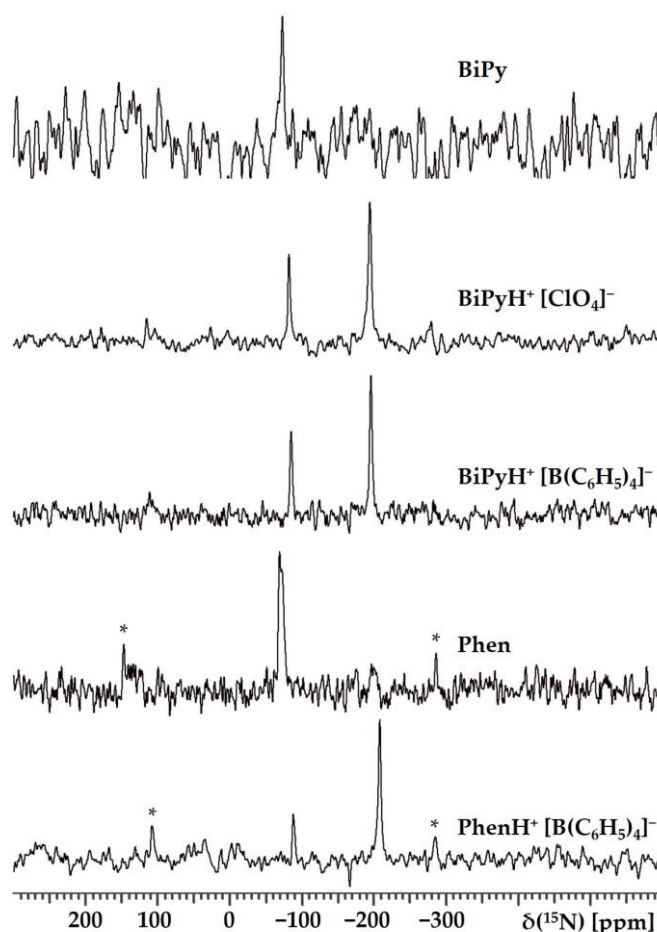
Figure 2. ^{15}N CPMAS NMR spectra of polycrystalline samples of BiPy, Phen, BiPyH$^+$, and PhenH$^+$. Asterisks * denote spinning sidebands.

Table 1. The experimental values of the isotropic ^{15}N chemical shift.

Substance	State	δ_{iso}, ppm
BiPy	Polycrystalline	−72.7
BiPy	In tetrahydrofuran	−71.65
BiPyH$^+$ [ClO$_4$]$^-$	Polycrystalline	−82.0 & −193.4
BiPyH$^+$ [B(C$_6$H$_5$)$_4$]$^-$	Polycrystalline	−85.0 & −195.5
Phen	Polycrystalline	−68.6 & −72.2
Phen	In tetrahydrofuran	−66.74
PhenH$^+$ [B(C$_6$H$_5$)$_4$]$^-$	Polycrystalline	−88.3 & −208.3

Hydrogen bonding significantly affects the $\delta_{iso}\left(^{15}N\right)$ of pyridines [38]. For symmetrically substituted pyridines, there is a functional dependence between the change in the $\delta_{iso}\left(^{15}N\right)$ and the value of the N . . . H distance [39]. This dependence was successfully used in the past to study the geometry of hydrogen bonds in complex molecular systems [40–42]. The maximal difference between the free and protonated forms is approximately the same for all pyridine derivatives and is 125 ppm [43].

The changes observed for BiPy and BiPyH$^+$, as well as for Phen and PhenH$^+$, are completely consistent with the expected changes (Table 1). The $\delta_{iso}\left(^{15}N\right)$ of the protonated nitrogen shifted to −200 ppm, while for the other, it changed by only −10 ppm. However, neither for BiPyH$^+$ nor for PhenH$^+$ could these changes be converted into the numerical values of the N-H and H . . . N distances using the mentioned dependence. The reasons for this limitation are as follows. (i) This dependence was established for linear hydrogen bonds. In BiPyH$^+$ and PhenH$^+$, these bonds are highly bent. (ii) The conformations of

BiPy and BiPyH$^+$ are different. (iii) In PhenH$^+$, the electron densities in the two conjugated pyridine rings cannot be considered independent. It is not known how these effects affect the values of the respective $\delta_{iso}(^{15}N)$. The geometry of the hydrogen bonds in these structures will have to be determined using theoretical calculations.

2.1.2. Calculated ^{15}N NMR Chemical Shifts

Non-covalent interactions cause changes in chemical shifts [44,45]. For solids, the theoretical evaluation of these changes requires either using the GIPAW approach [46–48] or fragment-based calculations [46,49,50]. Such calculations require knowledge of the exact crystal structure, which is not always available [51]. However, in many cases, the influence of intermolecular interactions is small, and the required accuracy is achieved using simple adducts or single-molecule calculations [52–54].

Figure 3 shows the notations for the selected distances and angles used in this work. The calculated structures discussed below are named S_FB_W_ωM. S stands for the structure. F and B stand for the DFT functional and the basis set used for geometry optimization. F = ω or T for ωB97XD and TPSSh. B = t or q for def2tzvp and def2qzvp. W stands for geometries optimized with the polarizable continuum model approximation (PCM) using SCRF=(Solvent=water). ω and M stand for the DFT functional (ωB97XD) and the basis set used for GIAO NMR calculations, M = t or q or S for def2tzvp, def2qzvp, and pcSseg-3.
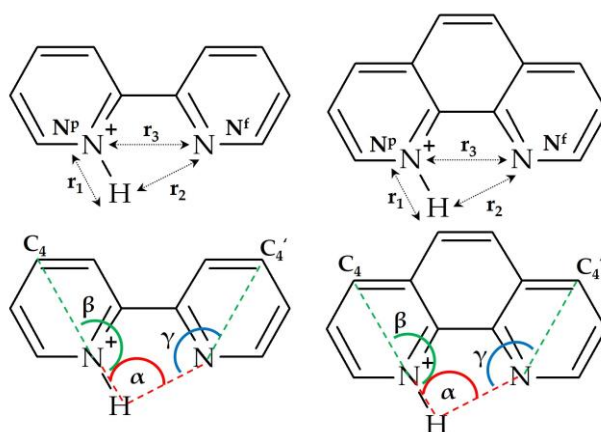

Figure 3. The notations for the selected distances and angles used in this work.

The structure BiPy_Tq_W_ωt was optimized using the TPSSh/def2qzvp approximation and SCRF=(Solvent=water). The $\delta_{iso}(^{15}N)$ values were calculated using the ωB97XD/def2qzvp approximation and SCRF=(Solvent=water). The selected geometric and NMR parameters for this structure are reported in Table 2. The numerical values of these parameters depend on the approximation used for geometry optimization but not on the approximation used for the NMR calculations; see the structures BiPy_Tq_W_ωq, BiPy_ωq_W_ωt, and BiPy_ωq_W_ωq. The $\delta_{iso}(^{15}N)$ values obtained for all these structures agree with the experimental values reported in Table 1. Therefore, the choice of the preferred approximation is a matter of taste.

BiPy*cis*_Tq_W_ωt corresponded to the *cis* form of BiPy, which is a higher-energy stable structure. The $\delta_{iso}(^{15}N)$ of this structure is somewhat different. Therefore, the functional dependence of the $\delta_{iso}(^{15}N)$ on the N . . . H distance found for pyridines [39] cannot be used for BiPy since it is not clear whether the chemical shift of the *cis* or *trans* conformer corresponds to the limit $N \ldots H \to \infty$.

BiPyH$^+$_Tq_W_ωt is the optimized structure of BiPyH$^+$. BiPyHClO$_4$_Tq_W_ωt is a structure in which the positions of all atoms, except for hydrogen atoms, were taken from the experimental XRD structure of BiPyH$^+$ [ClO$_4$]$^-$, while the hydrogen positions were optimized using the TPSSh/def2qzvp approximation and SCRF=(Solvent=water). ZUTDAT_Tq_W_ωt and ZUTDAT01_Tq_W_ωt were constructed in the same way using the experimental XRD structure of BiPyH$^+$ [B(C$_6$H$_5$)$_4$]$^-$ listed in the Cambridge Structural

Database under ID ZUTDAT [10] and ZUTDAT01 [55]. A comparison of the $\delta_{iso}\left(^{15}N\right)$ values for these structures suggests that they do not correlate unambiguously with the r_1 and r_2 distances. Of course, what is meant is not the obvious difference in the $\delta_{iso}\left(N^p\right)$ and $\delta_{iso}\left(N^f\right)$, but the variation in these values for different structures. These differences cannot be unambiguously attributed to the influence of the intramolecular hydrogen bond. Rather, they arose from differences in the geometries of these structures. On the other hand, protonation led to a significant decrease in the r_3 compared to BiPy*cis*_Tq_W_ωt.

Table 2. Calculated geometries and $\delta_{iso}\left(^{15}N\right)$ for the selected structures of BiPy and BiPyH$^+$.

Structure	r_1, Å	r_2, Å	r_3, Å	φ [1], °	δ_{iso}, ppm
BiPy_Tq_W_ωt	–	–	3.61234	180	−70
BiPy_Tq_W_ωq	–	–	3.61234	180	−70
BiPy_ωq_W_ωt	–	–	3.60001	180	−75
BiPy_ωq_W_ωq	–	–	3.60001	180	−74
BiPy*cis*_Tq_W_ωt	–	–	2.72141	0	−63
BiPyH$^+$_Tq_W_ωt	1.02483	2.05149	2.58497	0	−82 & −199
BiPyHClO$_4$_Tq_W_ωt	1.02871	2.24853	2.66167	14.6	−71 & −195
ZUTDAT_Tq_W_ωt	1.02365	2.08824	2.61085	4.3	−76 & −198
ZUTDAT01_Tq_W_ωt	1.02376	2.08657	2.60115	4.7	−82 & −202

[1] The dihedral angle between pyridine rings.

It is not a priori obvious which basis set is required for the correct computation of the $\delta_{iso}\left(^{15}N\right)$ of Phen. Three basis sets were used to calculate the $\delta_{iso}\left(^{15}N\right)$ of Phen structures optimized using the TPSSh/def2qzvp approximation and SCRF=(Solvent=water): Phen_Tq_W_ωt, Phen_Tq_W_ωq, and Phen_Tq_W_ωS (Table 3). All the basis sets gave the same value. OPENAN_Tt_W_ωt and OPENAN01_Tt_W_ωt are structures in which the positions of all atoms, except for hydrogen atoms, were taken from the experimental XRD structures of Phen listed in the Cambridge Structural Database under ID OPENAN [29] and OPENAN01 [30], while the hydrogen positions were optimized using the TPSSh/def2qzvp approximation and SCRF=(Solvent=water). There are two structurally distinct molecules in these crystal structures that have different $\delta_{iso}\left(^{15}N\right)$ values. The r_3 distances in the solid state were less than the calculated one. The calculated values of the $\delta_{iso}\left(^{15}N\right)$ approximately coincide, agree with the experimental values, and do not correlate with the r_3.

Table 3. Calculated geometries and $\delta_{iso}\left(^{15}N\right)$ for the selected structures of Phen and PhenH$^+$.

Structure	r_1, Å	r_2, Å	r_3, Å	δ_{iso}, ppm
Phen_Tq_W_ωt	–	–	2.77022	−67
Phen_Tq_W_ωq	–	–	2.77022	−68
Phen_Tq_W_ωS	–	–	2.77022	−67
OPENAN_Tt_W_ωt	–	–	2.72215	−65
			2.72614	−73
OPENAN01_Tt_W_ωt	–	–	2.73995	−65
			2.74499	−63
PhenH$^+$_Tq_W_ωt	1.02021	2.26272	2.70884	−84 & −207
ZUTDEX_Tq_W_ωt	1.01968	2.26295	2.70682	−81 & −204

Protonation resulted in a shortening of the r_3 distance. PhenH$^+$_Tq_W_ωt corresponded to the optimized structure of PhenH$^+$. ZUTDEX_Tq_W_ωt was constructed from the experimental XRD structure of PhenH$^+$ [B(C$_6$H$_5$)$_4$]$^−$ listed in the Cambridge Structural Database under ID ZUTDEX [10] in the same manner as described above. The calculated values of $\delta_{iso}\left(^{15}N\right)$ are similar and agree with the experimental values (Table 1).

The first objective of this work was achieved. The experimental and calculated values of the $\delta_{iso}\left(^{15}N\right)$ for BiPyH$^+$ and PhenH$^+$ agree quite well. Therefore, the calculated geometries of their intramolecular hydrogen bonds are reliable. Protonation resulted in

a shortening of the r_3 in both species. Although these distances are comparable to the shortest N ... N distance measured for the proton-bound homodimers of the pyridines of 2.62 Å [56,57], the intramolecular hydrogen bonds in BiPyH$^+$ and PhenH$^+$ are strongly bent. Their lengths should be calculated as $r_1 + r_2$, which gives about 3.08 Å and 3.28 Å, respectively. The difference between the $\delta_{iso}\left(^{15}N\right)$ in BiPy and Phen and the $\delta_{iso}\left(^{15}N\right)$ of the N-H nitrogens in BiPyH$^+$ and PhenH$^+$ is greater than 120 ppm, the value expected for an uncoordinated pyridinium [43]. Therefore, both the geometries and $\delta_{iso}\left(^{15}N\right)$ indicate that these hydrogen bonds are weak.

2.1.3. Hydrogen Bond Energy

What is the energy of the intramolecular hydrogen bonds in BiPyH$^+$ and PhenH$^+$? Given the chemical similarity of these cations to the proton-bound homodimer of pyridine (PyHPy$^+$), this energy can be estimated using simplified model calculations. Figure 4a shows the structure of PyHPy$^+$. This complex has been studied in detail in the past [56–65]. Its hydrogen bond is moderately strong, it is of the asymmetric N-H ... N type and exhibits fast reversible proton transfer in solution. Let us define the energy of the hydrogen bond in PyHPy$^+$, ΔE, as the difference between the electronic energy of PyHPy$^+$ for a given distance, r_2, and the sum of the electronic energies of pyridine and pyridinium. At the ωB97XD/def2tzvp approximation and SCRF=(Solvent=water), ΔE is minimal at r_2 = 1.645433 Å. This distance is longer than the experimental value of 1.532 Å [57]. The reason for this has been explained elsewhere [66,67]. As the r_2 increases, the ΔE increases and tends asymptotically to zero (Figure 4b). The numerical values are collected in Table S1 in the Supporting Information.
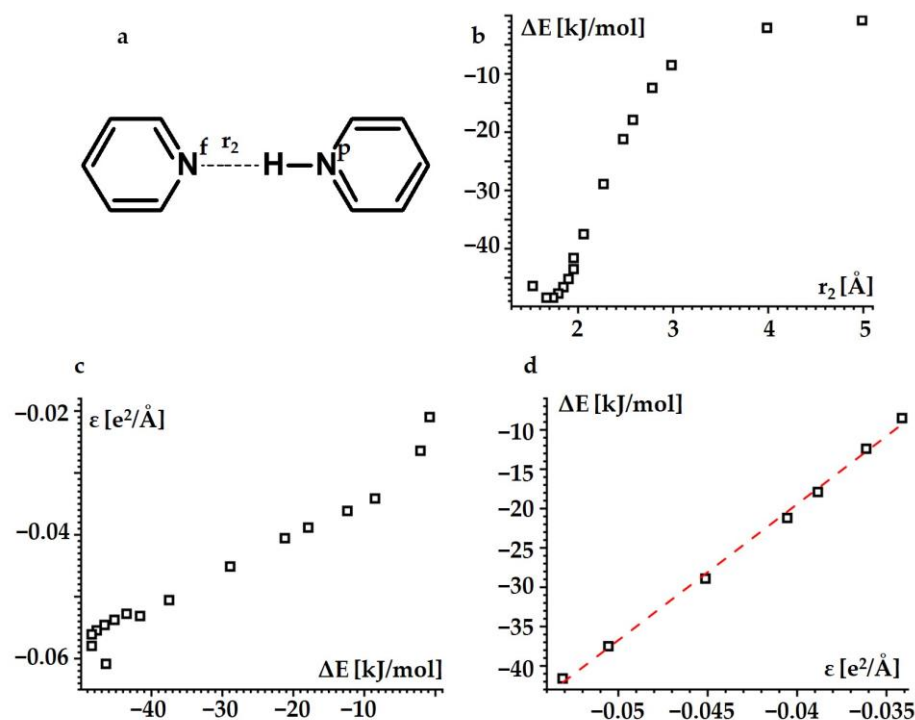

Figure 4. The hydrogen bond energy of PyHPy$^+$ estimated at the ωB97XD/def2tzvp approximation and SCRF=(Solvent=water). (**a**) The structure of PyHPy$^+$. (**b**) The hydrogen bond energy ΔE as a function of r_2. (**c**) The electric potential energy ε associated with the N^f ... H interaction as a function of ΔE. (**d**) The range of the linear dependence between ΔE and ε.

For a large r_2, one can expect that the binding energy of the hydrogen-bonded pyridine-N^p-H ... N^f-pyridine cation is defined by the electric force between the charges located at the N^f nitrogen and the binding proton. As an approximate numerical estimate of these charges, one can use the Mulliken charges of the N^f nitrogen $q(N^f)$ and the binding proton

$q(H)$. The electric potential energy associated with this interaction is $\varepsilon = q(H)q\left(N^f\right)/r_2$, where $q(H)$ and $q(N^f)$ are in units of the elementary charge e. Figure 4c shows ε as a function of the ΔE. For ΔE values between -41.6 kJ/mol and -8.5 kJ/mol, i.e., for r_2 values between 1.95 Å and 3.0 Å, a linear dependence between the ε and ΔE is evident. Thus, for this interval of the r_2 distances, the above assumption is correct. This dependence is $\Delta E = 1730 \cdot \varepsilon(\omega\text{B97XD}/\text{def2tzvp}) + 50$, where the ΔE is in kJ/mol and the ε in $e^2/\text{Å}$ (Figure 4d). (Of course, the energy of such hydrogen bonds can alternatively be defined as ε. In this case, however, there is ambiguity in the choice of the value of the relative permittivity, which requires additional assumptions that are difficult to justify.)

For the other approximations, the linearity of the dependence was preserved, but the numerical values of the coefficients changed. For the TPSSh/def2qzvp approximation, $\Delta E = 2720 \cdot \varepsilon(\text{TPSSh}/\text{def2qzvp}) + 98$ (Table S2). For the ωB97XD/def2qzvp approximation, $\Delta E = 2625 \cdot \varepsilon(\omega\text{B97XD}/\text{def2qzvp}) + 107$ (Table S3).

In BiPyH$^+$ and PhenH$^+$, the r_2 was in the range pf 2.0–2.3 Å. Thus, the obtained dependences could be used to estimate the hydrogen bond energy in these cations. The numerical values of ΔE varied depending on the basis set but were the same for the TPSSh and ωB97XD DFT functionals (Table 4). Consequently, the energy values of the intramolecular hydrogen bonds in BiPyH$^+$ and PhenH$^+$ were about 25 kJ/mol and 15 kJ/mol, respectively.

Table 4. The r_2 and r_3 distances, the Mulliken charges of the binding proton ($q(H)$) and the N^f nitrogen ($q(N^f)$), the electric potential energy ε, and the hydrogen bond energy ΔE in BiPyH$^+$ and PhenH$^+$ estimated at various approximations and SCRF=(Solvent=water).

Substance	r_2, Å	r_3, Å	$q(H)$, e	$q(N^f)$, e	ε [1], $e^2/\text{Å}$	ΔE, kJ/mol
BiPyH$^+$_wt_W	2.079695	2.595704	0.293915	-0.394282	-0.0557	-46 ± 3
BiPyH$^+$_Tq_W	2.051480	2.584967	0.255385	-0.362354	-0.0451	-25 ± 8
BiPyH$^+$_wq_W	2.080350	2.595114	0.237234	-0.446997	-0.0510	-27 ± 4
PhenH$^+$_wt_W	2.226297	2.688838	0.288186	-0.390619	-0.0506	-37 ± 3
PhenH$^+$_Tq_W	2.262717	2.708843	0.259246	-0.351045	-0.0402	-11 ± 8
PhenH$^+$_wq_W	2.273517	2.710015	0.246195	-0.424726	-0.0460	-14 ± 4

[1] The electric potential energy $\varepsilon = \frac{q(H)q(N^f)}{r_2}$ associated with the N^f ... H interaction.

2.2. Intramolecular Proton Transfer in BiPyH$^+$ and PhenH$^+$

Proton Transfer Pathway

This section discusses the theoretically modeled intramolecular proton transfer pathway in BiPyH$^+$ and PhenH$^+$. Since the exact numerical values of the considered geometric and energetic parameters are not the subject of this analysis, these calculations were carried out without using the PCM approximation. The proton transfer pathway was modeled as follows. The geometries of BiPyH$^+$ and PhenH$^+$ were optimized using the ωB97XD/def2tzvp approximation. Then, the r_1 distance was increased stepwise, and for each of the selected r_1 distances, the geometry was optimized again. The final structure, referred to below as a symmetric structure, corresponds to equal r_1 and r_2 distances. Thus, this model describes the case of proton transfer due to the gradual strengthening of the intramolecular hydrogen bond, in which the geometry of the molecule has time to adapt to this change. The resulting numerical values are reported in Tables S4 and S5.

Figure 5 shows the changes in the selected geometric parameters caused by such proton transfer. These changes are presented as functions of the proton coordinate $q_1 = \frac{1}{2}(r_1 - r_2)$. The decrease in q_1 caused a contraction of r_3 (Figure 5a). The trends of these changes were the same for BiPyH$^+$ and PhenH$^+$, although, in the latter, the r_3 was always longer by at least 0.05 Å. The changes in the angles α, β, and γ were the same as well (Figure 5b). Strengthening the hydrogen bond made it more linear, that is, the angle α increased. The convergence of the angles β and γ for a flexible BiPyH$^+$ occurred smoothly. On the contrary, for a rigid PhenH$^+$, the last step to $q_1 = 0$ caused a saltatory change in these angles.
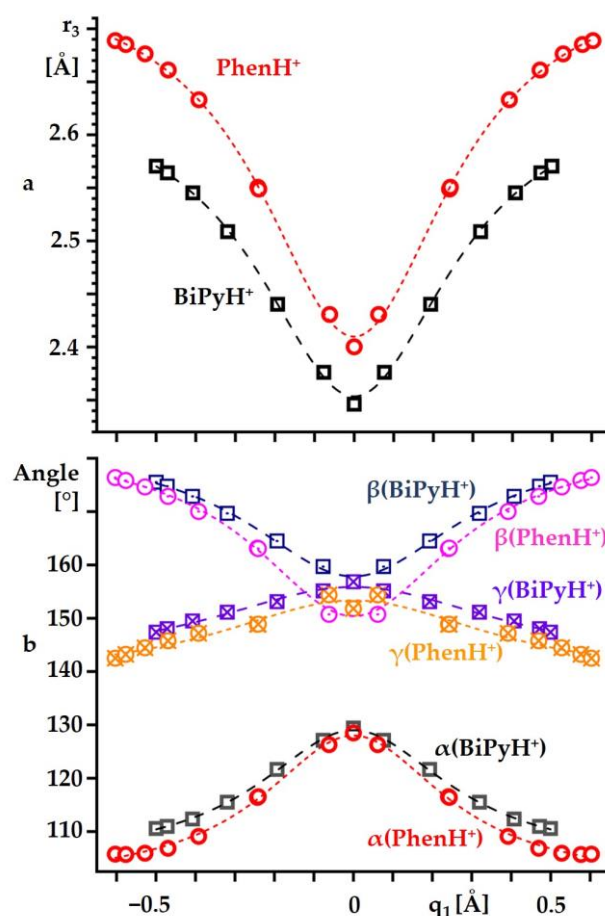
Figure 5. The changes in the r_3 (**a**) and selected angles (**b**) caused by the intramolecular proton transfer in BiPyH$^+$ and PhenH$^+$ as functions of the proton coordinate $q_1 = \frac{1}{2}(r_1 - r_2)$. Curves describe a trend and serve as a guide for the eyes.

Figure 6 shows the changes in the heavy atom hydrogen bond coordinate $q_2 = r_1 + r_2$ and the energy values of BiPyH$^+$ and PhenH$^+$ caused by such a proton transfer. As with any other known hydrogen bonds, the decrease in q_1 caused a contraction of q_2 [68–70] (Figure 6a). However, there was also a difference between the BiPyH$^+$ and PhenH$^+$. For a large q_1, the q_2 changed abnormally in PhenH$^+$ and somewhat increased with a decreasing q_1. This fact can be interpreted as an indication that, near the optimal geometry, the intramolecular hydrogen bond in PhenH$^+$ is weak and small changes in its geometry do not significantly affect the geometry of this rigid structure. On the contrary, in the limit of the strong hydrogen bonding at $q_1 = 0$, this bond was only slightly weaker than in BiPyH$^+$. Near the optimal geometry, a small increase in the r_1 did not cause a significant energy increase (Figure 6b). However, then the energy rapidly increased in an inverse proportion to q_1. For PhenH$^+$, this growth was much steeper than for BiPyH$^+$. As a result, the energies of the symmetric structures at $q_1 = 0$ were 41 kJ/mol and 72 kJ/mol higher than the energies of the lowest energy structures of BiPyH$^+$ and PhenH$^+$, respectively.

The energy required for the proton transfer, calculated above, is quite large. How much will this energy change if the polarity of the solvent is taken into account, SCRF=(Solvent=water)? The geometries of the lowest energy structures and the symmetric structures at $q_1 = 0$ of BiPyH$^+$ and PhenH$^+$ changed somewhat in this approximation (Tables S6 and S7). Their energy differences increased to 51 kJ/mol and 82 kJ/mol for BiPyH$^+$ and PhenH$^+$, respectively.
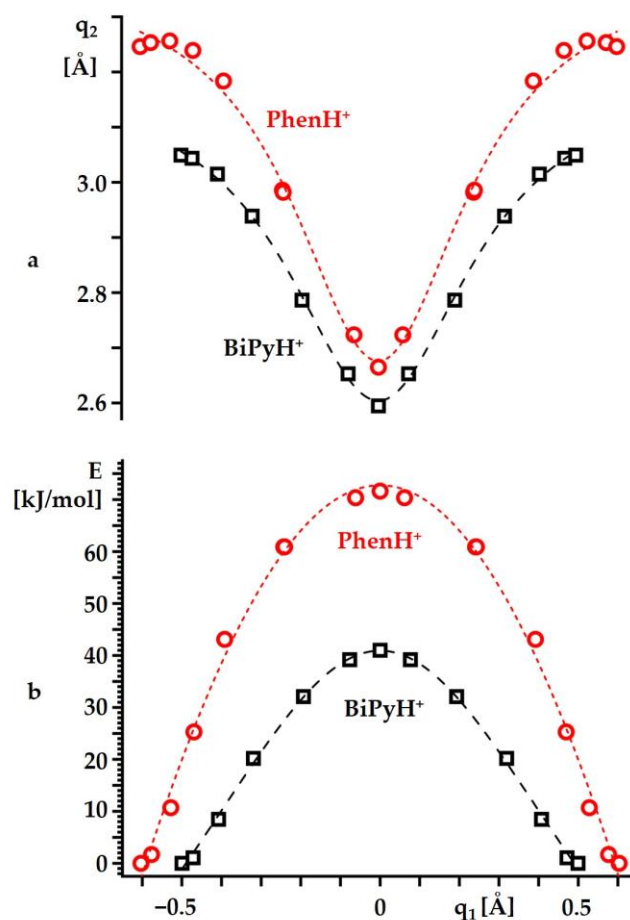
Figure 6. The changes in the heavy atom hydrogen bond coordinate $q_2 = r_1 + r_2$ (**a**) and the energy (**b**) caused by the proton transfer in BiPyH$^+$ and PhenH$^+$ as functions of $q_1 = \frac{1}{2}(r_1 - r_2)$. Curves describe a trend and serve as a guide for the eyes.

To obtain a more realistic estimate of the energy required for the proton transfer, the calculation procedure was changed. The geometries were optimized using the ωB97XD/def2tzvp approximation and SCRF=(Solvent=water). Then, the r_3 distance was decreased stepwise, and for each of the selected r_3 distances, the geometry was optimized. The final structure corresponded to equal r_1 and r_2 distances. For all these structures, the N^p-H stretches were calculated (Table S8). Thus, this model describes the case of proton transfer in which the movement of the proton is much faster than the ongoing changes in the r_3 distance and reduces the multi-dimensional potential energy problem [71–73] to a one-dimensional one. The only structure with a negative frequency is the structure with the equal r_1 and r_2 distances. Thus, these calculations show that no intramolecular vibrations can be the cause of the fast reversible proton transfer observed in BiPyH$^+$ in the experiment [9]. This process must be caused by external forces.

3. Materials and Methods

Solid-state ^{15}N NMR measurements were performed on an *Infinity$_{plus}$* spectrometer system (Varian Inc., Palo Alto, CA, USA) operated at 7 T and equipped with a Chemagnetics 6 mm pencil CPMAS probe. The ^{15}N{^{1}H} MAS CP NMR spectra were recorded using a $90°-$pulse length of 5.0 μsec, a cross-polarization contact time of 15 ms, and relaxation delays of 5–20 s. The spectra were indirectly referenced to CH$_3$NO$_2$ [74] using solid ^{15}NH$_4$Cl ($\delta = -341.3$ ppm [75]). To convert these values to the liquid ammonia scale, add 380.6 ppm to them [75].

The Gaussian 09.D.01 program package was used for geometry optimizations and NMR calculations [76]. The TPSSh and ωB97XD DFT hybrid functionals [77,78] and the def2tzvp, def2qzvp, and pcSseg-3 basis sets were used [79–81]. The geometry optimization was performed at the very tight convergence criteria. The NMR calculations were carried out using the GIAO approach. Some calculations were performed using the PCM approximation with water as the solvent [82]. This choice is arbitrary. The outcomes of the PCM approximation are not very sensitive to the value of the dielectric constant [83]. However, this correction is necessary to consider the effect of the crystal field.

To convert the ^{15}N NMR absolute shielding values σ obtained in the theoretical calculations into the chemical shift scale δ used in the experiments, it was necessary to know the reference ^{15}N absolute chemical shielding σ^{ref}: $\delta \approx \sigma^{ref} - \sigma$ [84,85]. The numerical value of σ^{ref} depends on the approximation used to calculate σ [86]. The calculated chemical shifts reported in this work were derived from the calculated absolute shielding values using the following values of σ^{ref}: $\sigma^{ref}(\omega$B97XD/def2tzvp$) = 143$ ppm, $\sigma^{ref}(\omega$B97XD/def2qzvp$) = 148$ ppm, and $\sigma^{ref}(\omega$B97XD/pcSseg3$) = 153$ ppm [86]. The applicability of this approach was previously confirmed for ^{31}P NMR [54,87,88].

Crystalline BiPyH$^+$ [ClO$_4$]$^-$ was obtained from a solution of 2,2'-bipyridine in tetrahydrofuran by adding 70% HClO$_4$. The precipitate was filtered off and recrystallized either from acetonitrile or from nitromethane. X−ray diffraction data for single crystals of BiPyH$^+$ [ClO$_4$]$^-$ were collected by Rigaku Oxford Diffraction SuperNova diffractometers (Tables S9 and S10, Applied Rigaku Technologies, Inc., Austin, TX, USA). The crystals were kept at 123.0 K during the data collection. The structures were solved with the ShelXT 2018/2 [89] solution program using dual methods and Olex2 1.5-alpha [90] as the graphical interface. The model was refined with Olex2.refine 1.5-alpha [91] using full matrix least squares minimization on F^2. The structures have been deposited at the Cambridge Crystallographic Data Centre (CCDC) with numbers 2266914 and 2266916. The atomic coordinates of the BiPyHClO4_Tq_W, ZUTDAT_Tq_W, ZUTDAT01_Tq_W, OPENAN_Tt_W, OPENAN01_Tt_W, and ZUTDEX_Tq_W structures are available in Tables S11–S16.

Polycrystalline BiPyH$^+$ [B(C$_6$H$_5$)$_4$]$^-$ and PhenH$^+$ [B(C$_6$H$_5$)$_4$]$^-$ were obtained from a solution of BiPy or Phen in methanol by adding 37% HCl and NaB(C$_6$H$_5$)$_4$. The precipitate was filtered off and washed with water.

4. Conclusions

This study had three objectives. First, it aimed to measure the ^{15}N NMR chemical shifts of BiPy, Phen, BiPyH$^+$, and PhenH$^+$ in the solid state and to compare these experimental values with theoretically calculated values to determine the correct hydrogen bond geometry in the condensed state. These measurements and calculations show equal results. Thus, the calculated geometries were similar to those of the solid state.

The second objective was to estimate the energy of the intramolecular hydrogen bond in BiPyH$^+$ and PhenH$^+$. The model calculations provided for the energy of these interactions were 25 kJ/mol and 15 kJ/mol, respectively. The nature of these hydrogen bonds is purely electrostatic. It would be instructive to make an independent estimate of these energies using the experimental electron density distribution function [92–96].

The final objective was to model the intramolecular proton transfer in BiPyH$^+$ and PhenH$^+$. The analysis showed that neither these interactions nor N-H stretches could be responsible for the fast reversible proton transfer observed for BiPyH$^+$ in a polar solvent down to 115 K. The electrostatic interaction between the mobile proton and the second nitrogen atom was a guide for the transfer, but it was too weak to overcome the transfer barrier. This process was controlled by an external force. This force was a fluctuating electric field present in the solution. Its effects and amplitude have been evaluated in the past for several molecular adducts [66,83,88,97,98]. However, the influence of this field on proton transfer can only be modeled if the transfer occurs along the symmetry axis of the adduct under consideration. Neither BiPyH$^+$ nor PhenH$^+$ has such an axis.

The particular results obtained for the examples of BiPyH[+] and PhenH[+] allow us to draw the following general conclusion. The hydrogen bonds under discussion are weak. By themselves, they could not have a significant effect on the properties of these molecules. However, these bonds are an integral part of a large system of interactions, which includes both intramolecular interactions and the influence of the environment. Within the framework of such a system, they become the grain that tips the scales.

References

1. Hynes, J.T.; Klinman, J.P.; Limbach, H.-H.; Schowen, R.L. *Hydrogen-Transfer Reachtions*; WILEY-VCH Verlag: Weinheim, Germany, 2007.
2. Kohen, A.; Limbach, H.-H. *Isotope Effects in Chemistry and Biology*; CRC Press: Boca Raton, FL, USA, 2006.
3. Howard, S.T. Conformers, Energetics, and Basicity of 2,2′-Bipyridine. *J. Am. Chem. Soc.* **1996**, *118*, 10269–10274. [CrossRef]
4. Merritt, L.L., Jr.; Schroeder, E.D. The crystal structure of 2,2′-bipyridine. *Acta Crystallogr.* **1956**, *9*, 801–804. [CrossRef]
5. Chisholm, M.H.; Huffman, J.C.; Rothwell, I.P.; Bradley, P.G.; Kress, N.; Woodruff, W.H. Bis(2,2′-bipyridyl)diisopropoxymolybdenum(II). Structural and Spectroscopic Evidence for Molybdenum-to-Bipyridyl π* Bonding. *J. Am. Chem. Soc.* **1981**, *103*, 4945–4947. [CrossRef]
6. Kühn, F.E.; Groarke, M.; Bencze, E.; Herdtweck, E.; Prazeres, A.; Santos, A.M.; Calhorda, M.J.; Romão, C.C.; Gonçalves, I.S.; Lopes, A.D.; et al. Octahedral Bipyridine and Bipyrimidine Dioxomolybdenum(vi) Complexes:Characterization, Application in Catalytic Epoxidation, and DensityFunctional Mechanistic Study. *Chem. Eur. J.* **2002**, *8*, 2370–2383. [CrossRef] [PubMed]
7. Cheng, C.L.; Murthy, D.S.N.; Ritchie, G.L.D. Molecular conformations from magnetic anisotropies. *J. Chem. Soc. Faraday Trans.* **1972**, *68*, 1679–1690. [CrossRef]
8. Lesnichin, S.B.; Kamdem, N.; Mauder, D.; Denisov, G.S.; Shenderovich, I.G. Studies of Adsorption of 2,2′-Bipyridyl on the Surface of Highly Regulated Silica Matrix of the MCM-41 Type by Means of ^{15}N NMR Spectroscopy. *Russ. J. Gen. Chem.* **2010**, *80*, 2027–2031. [CrossRef]
9. Lesnichin, S.B.; Tolstoy, P.M.; Limbach, H.-H.; Shenderovich, I.G. Counteranion-Dependent Mechanisms of Intramolecular Proton Transfer in Aprotic Solution. *Phys. Chem. Chem. Phys.* **2010**, *12*, 10373–10379. [CrossRef]
10. Bakshi, P.K.; Cameron, T.S.; Knop, O. Crystal chemistry of tetraradial species. Part 8. Mix and match: Cation geometry, ion packing, hydrogen bonding, and π–π interactions in cis-2,2′-bipyridinium(1+) and 1,10-phenanthrolinium(1+) tetraphenylborates—And what about proton sponges? *Can. J. Chem.* **1996**, *74*, 201–220. [CrossRef]
11. Schone, S.; Radoske, T.; Marz, J.; Stumpf, T.; Ikeda-Ohno, A. Synthesis and Characterization of Heterometallic Iron–Uranium Complexes with a Bidentate N-Donor Ligand (2,2′-Bipyridine or 1,10-Phenanthroline). *Inorg. Chem.* **2018**, *57*, 13318–13329. [CrossRef]
12. Kavitha, S.J.; Panchanatheswaran, K.; Low, N.J.; Glidewell, C. 2-(2-Pyridyl)pyridinium perchlorate, redetermined at 120 K: Complex hydrogen-bonded sheets. *Acta Crystallogr. Sect. C Cryst. Struct. Commun.* **2005**, *61*, o473–o474. [CrossRef]
13. Kadarkaraisamy, M.; Engelhart, D.P.; Basa, P.N.; Sykes, A.G. Hexafluorophosphate salts of bis and tetrakis(2,2′-bipyridine)lead(II) complexes. *J. Coord. Chem.* **2010**, *63*, 2261–2267. [CrossRef]
14. Milani, B.; Anzilutti, A.; Vicentini, L.; Sessanta o Santi, A.; Zangrando, E.; Geremia, S.; Mestroni, G. Bis-Chelated Palladium(II) Complexes with Nitrogen-Donor Chelating Ligands Are Efficient Catalyst Precursors for the CO/Styrene Copolymerization Reaction. *Organometallics* **1997**, *16*, 5064–5075. [CrossRef]
15. Kraus, F.; Breu, J. Arene-arene stacking in the revised structure of 2,2′-bipyridinium hexafluorophosphate. *Acta Crystallogr. Sect. C Cryst. Struct. Commun.* **2002**, *58*, o254–o256. [CrossRef] [PubMed]
16. Yoshikawa, N.; Yamazaki, S.; Kato, N.; Kubota, A.; Sawai, M.; Noda, K.; Kanehisa, N.; Inoue, T.; Nakata, E.; Takashima, H. Syntheses, X-Ray Crystal Structures, Emission Properties and DFT Calculations of Monoprotonated Polypyridines. *Chem. Sel.* **2019**, *4*, 59–65. [CrossRef]
17. Buttery, J.H.; Effendy; Junk,, P.C.; Mutrofin, S.; Skelton, B.W.; Whitaker, C.R.; White, A.H. The Structural Systematics of Protonation of Some Important Nitrogen-base Ligands. IV. Some Ethane-1,2-diaminium Univalent Anion Salt/1,10-Phenanthroline (Hydrate) Arrays. *Z. Anorg. Allg. Chem.* **2006**, *632*, 1326–1339. [CrossRef]
18. Jagan, R.; Sathya, D.; Sivakumar, K. A dihydrogen phosphate anionic network as a host lattice for cations in 1-methyl piperazine-1,4-diium bis (di hydrogen phosphate) and 2-(pyridin-2-yl)pyridinium di hydrogen phosphate-ortho phosphoric acid (1/1). *Acta Crystallogr. Sect. C Cryst. Struct. Chem.* **2015**, *71*, 374–380. [CrossRef]

19. Ivanova, B.; Spiteller, M. On the chemical identification and determination of flavonoids in solid-state. *Talanta* **2012**, *94*, 9–21. [CrossRef]

20. Charushnikova, I.A.; Den Auwer, C. 2,2′-Bipyridyl-2-ium aqua(2,2′-bipyridyl-$\kappa^2 N,N'$)-tetakis-(nitrato-$\kappa^2 O,O'$) -praseodymium(III) 2,2′-bipyridyl hemisolvate. *Acta Crystallogr. Sect. E Struct. Rep. Online* **2004**, *60*, m1775–m1777. [CrossRef]

21. Thuery, P. Sulfonate Complexes of Actinide Ions: Structural Diversity in Uranyl Complexes with 2-Sulfobenzoate. *Inorg. Chem.* **2013**, *52*, 435–447. [CrossRef]

22. Mrvos-Sermek, D.; Popovic, Z.; Matkovic-Calogovic, D. Hydrogen Bonding in the 2,2′-Bipyridinium Salt of 1,2,4,5-Benzenetetracarboxylic Acid (Pyromellitic Acid). *Acta Crystallogr. Sect. C Cryst. Struct. Commun.* **1996**, *52*, 2538–2541. [CrossRef]

23. Thuery, P. 2,2′-Bipyridine and 1,10-Phenanthroline as Coligands or Structure-Directing Agents in Uranyl–Organic Assemblies with Polycarboxylic Acids. *Eur. J. Inorg. Chem.* **2013**, *2013*, 4563–4573. [CrossRef]

24. Jurowska, A.; Szklarzewicz, J.; Basta, N.; Hodorowicz, M. Structural and physicochemical characterization of ion-pair salts with dipyridyl cations and $[Fe(CN)_6]^{4-}$ and $[Fe(CN)_5(NO)]^{2-}$ anions. *Inorg. Chim. Acta* **2022**, *539*, 121033. [CrossRef]

25. Balabanova, S.P.; Buikin, P.A.; Ilyukhin, A.B.; Rudenko, A.Y.; Dorovatovskii, P.V.; Korlyukov, A.A.; Kotov, V.Y. Crystal Structure and Optical Properties of New Hybrid Halobismuthates of 2,2′-Bipyridinium Derivatives. *Russ. J. Inorg. Chem.* **2022**, *67*, 1018–1024. [CrossRef]

26. Jurowska, A.; Szklarzewicz, J.; Hodorowicz, M. Ion pair charge-transfer salts based on protonated bipyridines and $[W(CN)_6(bpy)]^{2-}$ anion-structure and properties. *J. Mol. Struct.* **2022**, *1261*, 132931. [CrossRef]

27. Summers, L.A. The Bipyridines. *Adv. Heterocycl. Chem.* **1984**, *35*, 281–374. [CrossRef]

28. Vogler, A.; Shenderovich, I.G. Photochemistry of deprotonated rhenium(I) (3,3′-dihydroxy-2,2′-bipyridine) tricarbonyl chloride. Photoisomerization at the chelate in basic solution. *Inorg. Chim. Acta* **2014**, *421*, 496–499. [CrossRef]

29. Nishigaki, S.; Yoshioka, H.; Nakatsu, K. The crystal and molecular structure of o-phenanthroline. *Acta Crystallogr. Sect. B Struct. Crystallogr. Cryst. Chem.* **1978**, *34*, 875–879. [CrossRef]

30. Gembicky, M. The Cambridge Structural Database Communication ID OPENAN01. University of Buffalo: Buffalo, NY, USA, 2020.

31. Rojas, Y.; Tadrosse, M.; Assaf, C.; Bernal, I.; Lalancette, R.A. Preparation and structural studies of manganese polychloride anions in three metal charge states [((II), (III), (IV)]—Their stereochemistries. *Struct. Chem.* **2020**, *31*, 1309–1316. [CrossRef]

32. Oswald, I.W.H.; Ahn, H.; Neilson, J.R. Influence of organic cation planarity on structural templating in hybrid metal-halides. *Dalton Trans.* **2019**, *48*, 16340–16349. [CrossRef]

33. Gel'mbol'dt, V.O.; Anisimov, V.Y.; Fonar', M.S. Interaction between hydrofluorosilicic acid and 1,10-phenanthroline: Hydrolytic stability of chelate complexes of silicon tetrafluoride with bidentate N-donors. *Russ. J. Inorg. Chem.* **2016**, *61*, 822–825. [CrossRef]

34. Ma, G.; Ilyukhin, A.; Glaser, J. 2,2′-Bipyridinium bis(perchlorate). *Acta Crystallogr. Sect. C Cryst. Struct. Chem.* **2000**, *C56*, 1473–1475. [CrossRef] [PubMed]

35. Bujak, M.; Frank, W. Crystal structure of 1,10-phenanthrolindiium bis(triiodide) monohydrate, $C_{12}H_{12}I_6N_2O$. *Z. Kristallogr. -New Cryst. Struct.* **2014**, *229*, 379–380. [CrossRef]

36. Li, F.; Yin, H.; Simpson, J. *catena*-Poly[1,10-phen anthroline-1,10-diium [[dichlorido bismuthate(III)]-di-μ-chlorido]]. *Acta Crystallogr. Sect. E Struct. Rep. Online* **2007**, *63*, m1746. [CrossRef]

37. Pelties, S.; Maier, T.; Herrmann, D.; de Bruin, B.; Rebreyend, C.; Gärtner, S.; Shenderovich, I.G.; Wolf, R. Selective P_4 Activation by a Highly Reduced Cobaltate: Synthesis of Dicobalt Tetraphosphido Complexes. *Chem. Eur. J.* **2017**, *23*, 6094–6102. [CrossRef] [PubMed]

38. Solum, M.S.; Altmann, K.L.; Strohmeier, M.; Berges, D.A.; Zhang, Y.; Facelli, J.C.; Pugmire, R.J.; Grant, D.M. ^{15}N Chemical Shift Principal Values in Nitrogen Heterocycles. *J. Am. Chem. Soc.* **1997**, *119*, 9804–9809. [CrossRef]

39. Lorente, P.; Shenderovich, I.G.; Golubev, N.S.; Denisov, G.S.; Buntkowsky, G.; Limbach, H.-H. ^{1}H/^{15}N NMR Chemical Shielding, Dipolar ^{15}N, ^{2}H Coupling and Hydrogen Bond Geometry Correlations in a Novel Series of Hydrogen-Bonded Acid–Base Complexes of Collidine with Carboxylic Acids. *Magn. Reson. Chem.* **2001**, *39*, S18–S29. [CrossRef]

40. Brilmayer, R.; Brodrecht, M.; Kaiser, C.; Breitzke, H.; Kumari, B.; Wachtveitl, J.; Buntkowsky, G.; Andrieu-Brunsen, A. The Interplay of Nanoconfinement and pH from the Perspective of a Dye-Reporter Molecule. *ChemNanoMat* **2020**, *6*, 1843–1853. [CrossRef]

41. Sharif, S.; Denisov, G.S.; Toney, M.D.; Limbach, H.-H. NMR Studies of Solvent-Assisted Proton Transfer in a Biologically Relevant Schiff Base: Toward a Distinction of Geometric and Equilibrium H-Bond Isotope Effects. *J. Am. Chem. Soc.* **2006**, *128*, 3375–3387. [CrossRef]

42. Tupikina, E.Y.; Sigalov, M.V.; Tolstoy, P.M. Simultaneous Estimation of Two Coupled Hydrogen Bond Geometries from Pairs of Entangled NMR Parameters: The Test Case of 4-Hydroxypyridine Anion. *Molecules* **2022**, *27*, 3923. [CrossRef]

43. Andreeva, D.V.; Ip, B.; Gurinov, A.A.; Tolstoy, P.M.; Shenderovich, I.G.; Limbach, H.-H. Geometrical Features of Hydrogen Bonded Complexes Involving Sterically Hindered Pyridines. *J. Phys. Chem. A* **2006**, *110*, 10872–10879. [CrossRef]

44. Li, Z.J.; Abramov, Y.; Bordner, J.; Leonard, J.; Medek, A.; Trask, A.V. Solid-State Acid−Base Interactions in Complexes of Heterocyclic Bases with Dicarboxylic Acids: Crystallography, Hydrogen Bond Analysis, and 15N NMR Spectroscopy. *J. Am. Chem. Soc.* **2006**, *128*, 8199–8210. [CrossRef] [PubMed]

45. Gorobets, N.; Yermolayev, S.A.; Gurley, T.; Gurinov, A.A.; Tolstoy, P.M.; Shenderovich, I.G.; Leadbeater, N.E. Difference between 1H NMR signals of primary amide protons as a simple spectral index of the amide intramolecular hydrogen bond strength. *J. Phys. Org. Chem.* **2012**, *25*, 287–295. [CrossRef]

46. Hartman, J.D.; Harper, J.K. Improving the accuracy of GIPAW chemical shielding calculations with cluster and fragment corrections. *Solid State Nucl. Magn. Reson.* **2022**, *122*, 101832. [CrossRef]

47. Stevens, J.S.; Byard, S.J.; Seaton, C.C.; Sadiq, G.; Daveya, R.J.; Schroeder, S.L.M. Proton transfer and hydrogen bonding in the organic solid state: A combined XRD/XPS/ssNMR study of 17 organic acid–base complexes. *Phys. Chem. Chem. Phys.* **2014**, *16*, 1150–1160. [CrossRef]

48. Tatton, A.S.; Blade, H.; Brown, S.P.; Hodgkinson, P.; Hughes, L.P.; Lill, S.O.N.; Yates, J.R. Improving Confidence in Crystal Structure Solutions Using NMR Crystallography: The Case of β-Piroxicam. *Cryst. Growth Des.* **2018**, *18*, 3339–3351. [CrossRef]

49. Chernyshov, I.Y.; Vener, M.V.; Shenderovich, I.G. Local-structure effects on 31P NMR chemical shift tensors in solid state. *J. Chem. Phys.* **2019**, *150*, 144706. [CrossRef] [PubMed]

50. Hartman, J.D.; Kudla, R.A.; Day, G.M.; Mueller, L.J.; Beran, G.J.O. Benchmark fragment-based 1H, 13C, 15N and 17O chemical shift predictions in molecular crystals. *Phys. Chem. Chem. Phys.* **2016**, *18*, 21686–21709. [CrossRef] [PubMed]

51. Kleemiss, F.; Dolomanov, O.V.; Bodensteiner, M.; Peyerimhoff, N.; Midgley, L.; Bourhis, L.J.; Genoni, A.; Malaspina, L.A.; Jayatilaka, D.; Spencer, J.L.; et al. Accurate crystal structures and chemical properties from NoSpherA2. *Chem. Sci.* **2021**, *12*, 1675–1692. [CrossRef]

52. Ludwig, M.; Himmel, D.; Hillebrecht, H. GIAO versus GIPAW: Comparison of Methods To Calculate 11B NMR Shifts of Icosahedral *Closo*-Heteroboranes toward Boron-Rich Borides. *J. Phys. Chem. A* **2020**, *124*, 2173–2185. [CrossRef]

53. Shenderovich, I.G. Qualitative Analysis of the Geometry of the Hydrogen Bond in the Homoconjugated Pyridine Ion. *Russ. J. Gen. Chem.* **2007**, *77*, 620–625. [CrossRef]

54. Shenderovich, I.G. Experimentally Established Benchmark Calculations of ^{31}P NMR Quantities. *Chem.—Methods* **2021**, *1*, 61–70. [CrossRef]

55. Light, M.E.; Murphy, B. *The Cambridge Structural Database Communication ID ZUTDAT01*; University of Southampton: Southampton, UK, 2018.

56. Gurinov, A.A.; Lesnichin, S.B.; Limbach, H.-H.; Shenderovich, I.G. How short is the Strongest Hydrogen Bond in the Proton-Bound Homodimers of Pyridine Derivatives? *J. Phys. Chem. A* **2014**, *118*, 10804–10812. [CrossRef] [PubMed]

57. Kong, S.; Borissova, A.O.; Lesnichin, S.B.; Hartl, M.; Daemen, L.L.; Eckert, J.; Antipin, M.Y.; Shenderovich, I.G. Geometry and Spectral Properties of the Protonated Homodimer of Pyridine in the Liquid and Solid States. A Combined NMR, X-ray Diffraction and Inelastic Neutron Scattering Study. *J. Phys. Chem. A* **2011**, *115*, 8041–8048. [CrossRef] [PubMed]

58. Chan, B.; Del Bene, J.E.; Radom, L. What factors determine whether a proton-bound homodimer has a symmetric or an asymmetric hydrogen bond? *Mol. Phys.* **2009**, *107*, 1095–1105. [CrossRef]

59. Mori, Y.; Takano, K. Location of protons in N–H···N hydrogen-bonded systems: A theoretical study on intramolecular pyridine–dihydropyridine and pyridine–pyridinium pairs. *Phys. Chem. Chem. Phys.* **2012**, *14*, 11090–11098. [CrossRef]

60. Melikova, S.M.; Rutkowski, K.S.; Gurinov, A.A.; Denisov, G.S.; Rospenk, M.; Shenderovich, I.G. FTIR study of the hydrogen bond symmetry in protonated homodimers of pyridine and collidine in solution. *J. Mol. Struct.* **2012**, *1018*, 39–44. [CrossRef]

61. Hakkert, S.B.; Erdélyi, M. Halogen bond symmetry: The N-X-N bond. *J. Phys. Org. Chem.* **2015**, *28*, 226–233. [CrossRef]

62. Mori, Y.; Takano, K. Effect of solvent on proton location and dynamic behavior in short intramolecular hydrogen bonds studied by molecular dynamics simulations and NMR experiments. *Chem. Phys.* **2015**, *458*, 18–29. [CrossRef]

63. Gurinov, A.A.; Denisov, G.S.; Borissova, A.O.; Goloveshkin, A.S.; Greindl, J.; Limbach, H.-H.; Shenderovich, I.G. NMR Study of Solvation Effect on the Geometry of Proton-Bound Homodimers of Increasing Size. *J. Phys. Chem. A* **2017**, *121*, 8697–8705. [CrossRef]

64. Reiersølmoen, A.C.; Battaglia, S.; Øien-Ødegaard, S.; Gupta, A.K.; Fiksdahl, A.; Lindh, R.; Erdélyi, M. Symmetry of three-center, four-electron bonds. *Chem. Sci.* **2020**, *11*, 7979–7990. [CrossRef]

65. Grabowski, S.J. Hydrogen Bond and Other Lewis Acid-Lewis Base Interactions as Preliminary Stages of Chemical Reactions. *Molecules* **2020**, *25*, 4668. [CrossRef] [PubMed]

66. Shenderovich, I.G.; Denisov, G.S. Adduct under Field—A Qualitative Approach to Account for Solvent Effect on Hydrogen Bonding. *Molecules* **2020**, *25*, 436. [CrossRef] [PubMed]

67. Shenderovich, I.G. Actual Symmetry of Symmetric Molecular Adducts in the Gas Phase, Solution and in the Solid State. *Symmetry* **2021**, *13*, 756. [CrossRef]

68. Steiner, T. Lengthening of the Covalent X-H Bond in Heteronuclear Hydrogen Bonds Quantified from Organic and Organometallic Neutron Crystal Structures. *J. Phys. Chem. A* **1998**, *102*, 7041–7052. [CrossRef]

69. Steiner, T. The Hydrogen Bond in the Solid State. *Angew. Chem. Int. Ed.* **2002**, *41*, 48–76. [CrossRef]

70. Limbach, H.-H.; Tolstoy, P.M.; Pérez-Hernández, N.; Guo, J.; Shenderovich, I.G.; Denisov, G.S. OHO Hydrogen Bond Geometries and NMR Chemical Shifts: From Equilibrium Structures to Geometric H/D Isotope Effects, with Applications for Water, Protonated Water, and Compressed Ice. *Israel J. Chem.* **2009**, *49*, 199–216. [CrossRef]

71. Shibl, M.F.; Pietrzak, M.; Limbach, H.-H.; Kühn, O. Geometric H/D isotope effects and cooperativity of the hydrogen bonds in porphycene. *ChemPhysChem* **2007**, *8*, 315–321. [CrossRef]

72. Yamamoto, K.; Kanematsu, Y.; Nagashima, U.; Ueda, A.; Mori, H.; Tachikawa, M. Theoretical study of the H/D isotope effect on phase transition of hydrogen-bonded organic conductor κ-H$_3$(Cat-EDT-TTF)$_2$. *Phys. Chem. Chem. Phys.* **2016**, *18*, 29673–29680. [CrossRef]

73. Golubev, N.S.; Melikova, S.M.; Shchepkin, D.N.; Shenderovich, I.G.; Tolstoy, P.M.; Denisov, G.S. Interpretation of H/D Isotope Effects on NMR Chemical Shifts of [FHF]$^-$ Ion Based on Calculations of Nuclear Magnetic Shielding Tensor Surface. *Z. Phys. Chem.* **2003**, *217*, 1549–1563. [CrossRef]

74. Harris, R.K.; Becker, E.D.; Cabral De Menezes, S.M.; Granger, P.; Hoffman, R.E.; Zilm, K.W. Further conventions for NMR shielding and chemical shifts IUPAC recommendations 2008. *Solid State Nucl. Magn. Reson.* **2008**, *33*, 41–56. [CrossRef]

75. Bertani, P.; Raya, J.; Bechinger, B. ^{15}N chemical shift referencing in solid state NMR. *Solid State Nucl. Magn. Reson.* **2014**, *61–62*, 15–18. [CrossRef] [PubMed]

76. Frisch, M.J.; Trucks, G.W.; Schlegel, H.B.; Scuseria, G.E.; Robb, M.A.; Cheeseman, J.R.; Scalmani, G.; Barone, V.; Petersson, G.A.; Nakatsuji, H.; et al. *Gaussian 09*; Revision D.01; Gaussian, Inc.: Wallingford, CT, USA, 2013.

77. Staroverov, V.N.; Scuseria, G.E.; Tao, J.; Perdew, J.P. Comparative assessment of a new nonempirical density functional: Molecules and hydrogen-bonded complexes. *J. Chem. Phys.* **2003**, *119*, 12129. [CrossRef]

78. Chai, J.-D.; Head-Gordon, M. Long-range corrected hybrid density functionals with damped atom–atom dispersion corrections. *Phys. Chem. Chem. Phys.* **2008**, *10*, 6615–6620. [CrossRef] [PubMed]

79. Weigend, F.; Ahlrichs, R. Balanced basis sets of split valence, triple zeta valence and quadruple zeta valence quality for H to Rn: Design and assessment of accuracy. *Phys. Chem. Chem. Phys.* **2005**, *7*, 3297–3305. [CrossRef] [PubMed]

80. Jensen, F. Segmented Contracted Basis Sets Optimized for Nuclear Magnetic Shielding. *J. Chem. Theory Comput.* **2015**, *11*, 132–138. [CrossRef]

81. Pritchard, B.P.; Altarawy, D.; Didier, B.; Gibson, T.D.; Windus, T.L. New Basis Set Exchange: An Open, Up-to-Date Resource for the Molecular Sciences Community. *J. Chem. Inf. Model.* **2019**, *59*, 4814–4820. [CrossRef]

82. Tomasi, J.; Mennucci, B.; Cammi, R. Quantum mechanical continuum solvation models. *Chem. Rev.* **2005**, *105*, 2999–3093. [CrossRef]

83. Shenderovich, I.G. Simplified Calculation Approaches Designed to Reproduce the Geometry of Hydrogen Bonds in Molecular Complexes in Aprotic Solvents. *J. Chem. Phys.* **2018**, *148*, 124313. [CrossRef]

84. Bryce, D.L.; Bernard, G.M.; Gee, M.; Lumsden, M.D.; Eichele, K.; Wasylishen, R.E. Practical Aspects of Modern Routine Solid-State Multinuclear Magnetic Resonance Spectroscopy: One-Dimensional Experiments. *Can. J. Anal. Sci. Spectrosc.* **2001**, *46*, 46–82. Available online: http://anorganik.uni-tuebingen.de/klaus/nmr/practical/practical.pdf (accessed on 4 June 2023). [CrossRef]

85. Shenderovich, I.G.; Limbach, H.-H. Solid State NMR for Nonexperts: An Overview of Simple but General Practical Methods. *Solids* **2021**, *2*, 139–154. [CrossRef]

86. Shenderovich, I.G. An Experimentally Established ^{15}N NMR Absolute Shielding Scale for Theoretical Calculations. *J. Phys. Chem. A* **2023**. [CrossRef]

87. Shenderovich, I.G. 1,3,5-Triaza-7-Phosphaadamantane (PTA) as a ^{31}P NMR Probe for Organometallic Transition Metal Complexes in Solution. *Molecules* **2021**, *26*, 1390. [CrossRef]

88. Shenderovich, I.G. Electric field effect on ^{31}P NMR magnetic shielding. *J. Chem. Phys.* **2020**, *153*, 184501. [CrossRef]

89. Sheldrick, G.M. ShelXT-Integrated space-group and crystal-structure determination. *Acta Crystallogr. Sect. A Found. Adv.* **2015**, *A71*, 3–8. [CrossRef] [PubMed]

90. Dolomanov, O.V.; Bourhis, L.J.; Gildea, R.J.; Howard, J.A.K.; Puschmann, H. Olex2: A complete structure solution, refinement and analysis program. *J. Appl. Cryst.* **2009**, *42*, 339–341. [CrossRef]

91. Bourhis, L.J.; Dolomanov, O.V.; Gildea, R.J.; Howard, J.A.K.; Puschmann, H. The Anatomy of a Comprehensive Constrained, Restrained, Refinement Program for the Modern Computing Environment—Olex2 Disected. *Acta Crystallogr. Sect. A Found. Adv.* **2015**, *A71*, 59–71. [CrossRef]

92. Ananyev, I.V.; Lyssenko, K.A. Conjugation effects in a para-nitroaniline molecule and its structural non-rigidity. *Russ. Chem. Bull.* **2014**, *63*, 1270–1282. [CrossRef]

93. Borissova, A.O.; Lyssenko, K.A.; Gurinov, A.A.; Shenderovich, I.G. Energy Analysis of Competing Non-Covalent Interaction in 1:1 and 1:2 Adducts of Collidine with Benzoic Acids by Means of X-Ray Diffraction. *Z. Phys. Chem.* **2013**, *227*, 775–790. [CrossRef]

94. Vologzhanina, A.V.; Lyssenko, K.A. Interatomic interactions in the crystal of $(C_4H_{11}N_2)_2(C_4H_{12}N_2)[Mo(CN)_8]$: Comparison of two approaches. *Russ. Chem. Bull.* **2013**, *64*, 1786–1792. [CrossRef]

95. Nelyubina, Y.V.; Glukhov, I.V.; Antipin, M.Y.; Lyssenko, K.A. Higher density does not mean higher stability" mystery of paracetamol finally unraveled. *Chem. Commun.* **2010**, *46*, 3469–3471. [CrossRef]

96. Nelyubina, Y.V.; Antipin, M.Y.; Lyssenko, K.A. Hydrogen Bonds between Zwitterions: Intermediate between Classical and Charge-Assisted Ones. A Case Study. *J. Phys. Chem. A* **2009**, *113*, 3615–3620. [CrossRef] [PubMed]

97. Shenderovich, I.G.; Denisov, G.S. Modeling of the Response of Hydrogen Bond Properties on an External Electric Field: Geometry, NMR Chemical Shift, Spin-Spin Scalar Coupling. *Molecules* **2021**, *26*, 4967. [CrossRef] [PubMed]

98. Shenderovich, I.G.; Denisov, G.S. Modeling of Solute-Solvent Interactions Using an External Electric Field—From Tautomeric Equilibrium in Nonpolar Solvents to the Dissociation of Alkali Metal Halides. *Molecules* **2021**, *26*, 1283. [CrossRef] [PubMed]